

Water Vapor Production by Solar Radiation in a Short Circuit Using a Compound Parabolic Trough Concentrator (CPC)

Souleymane Ouedraogo^{1,*}, Sampawinde Augustin Zongo¹, Jean-Fidele Nzihou^{1,2}, Tizane Daho¹, Antoine Bere¹, Bila Gerard Segda¹

¹Laboratory of Environmental Physics and Chemistry, Joseph Ki-Zerbo University, Ouagadougou, Burkina Faso

²Laboratory of Energetic Research and Space Meteorology, Norbert Zongo University, Koudougou, Burkina Faso

Email address:

souley1010@yahoo.fr (Souleymane O.), zongosaugustin@yahoo.fr (Sampawinde A. Z.), jeanfidele@hotmail.com (Jean-Fidele N.), tizane_daho@yahoo.fr (Tizane D.), berebiya@yahoo.fr (Antoine B.), gsegda@gmail.com (Bila G. S.)

*Corresponding author

To cite this article:

Souleymane Ouedraogo, Sampawinde Augustin Zongo, Jean-Fidele Nzihou, Tizane Daho, Antoine Bere, Bila Gerard Segda. Water Vapor Production by Solar Radiation in a Short Circuit Using a Compound Parabolic Trough Concentrator (CPC). *American Journal of Energy Engineering*. Vol. 10, No. 2, 2022, pp. 35-44. doi: 10.11648/j.ajee.20221002.12

Received: March 24, 2022; **Accepted:** April 21, 2022; **Published:** April 28, 2022

Abstract: In this paper water vapor is directly generate in a short circuit by means of a compound parabolic trough concentrator (CPC) while optimizing the manufacturing costs of the solar device used. Direct steam generation has been widely studied, especially for high power systems. However, experimental applications for small solar field areas are rare, especially for concentrating solar technology. This research shows that it is possible to produce water vapor with a CPC for cooking, dry cleaning, maintenance and cleaning, etc. The different heat exchanges that took place in each compartment of the CPC were described. The heat transfer equations were solved by the Gauss-Seidel's method. An advanced difference scheme is used for the storage terms and a decentered scheme for the transport terms. The numerical simulation has been implemented by matlab code. The different CPC parameters have been directly measure experimentally. The results show that for a CPC length $L_c=1$ meter and width $l_c=50$ centimeter, the theoretical temperatures of the water and the absorber can reach 125°C and 150°C respectively, while the experimental temperatures of the water and the absorber are 108°C and 112°C respectively. The temperature of the water vapor measured can reach 110°C. The mass of water vapor produced with this device is 0.110 Kg with a mass flow rate of 3×10^{-6} Kg/s and a saturating vapor pressure of 1.05 bar. The theoretical thermal efficiency reached is 52% against an experimental value of 35% for a global solar radiation of 950 W/m² and an ambient temperature of 43°C at solar noon in April 2021. The CPC is designed to operate only during the day, and we are planning to add a heat storage system to our CPC for night use of the steam produced. In addition, instead of water, we can test the CPC's operation in the future with vegetable oils such as moringa oil.

Keywords: CPC, Water Vapor, Mass, Mass Flow Rate, Temperature, Pressure

1. Introduction

In most African countries, economic growth leads to significant and increasing energy needs [1, 2]. The inaccessibility of energy resources inevitably constitutes a major obstacle to economic growth. The galloping inflation of raw material and fossil fuel prices further weakens the economies of African countries whose industrial units are heavily and predominantly dependent on this type of energy.

Burkina Faso, a Sahelian country in the heart of West Africa with a national electrification rate estimated at 17% in 2014, 4% of which is in rural areas, is facing an energy demand due to the development of economic activities and population growth [3]. According to the Tableau de Bord 2017 of the Ministry of Energy, the share of fossil fuels in primary energy consumption in Burkina Faso is 88%. The remainder comes from renewable resources (hydropower 11%) and solar photovoltaic (1%) [4].

Since 2015, Burkina Faso yearly energy importation has been on an upward trend. This increase, which was 2.5% in 2017 compared to 2016, represents an average of 35% of the electricity supply over the period 2008-2017 [4]. Most of the energy imported come from Ivory Coast with 90% in 2017 [4]. These imports help meet part of the population's electricity demand. This situation has a negative impact on the local and national economy, lead energy dependency on exporting countries, which weakens our country's energy sector, as it is subject to external hazards such as supply chain disruptions and increased resource and transport costs.

Faced with these difficulties and in order to initiate an energy transition of our country towards its self-sufficiency to achieve a reasonable and sustainable energy solution to explore all forms of existing and available energy, to diversify the sources of energy production. That passes for some years, to the development of renewable energies to face the fluctuations of the prices of hydrocarbons and to reduce the emissions of greenhouse gases. Among the renewable energies, concentrated thermodynamic solar power is another process for producing electricity from solar energy. Like many sub-Saharan African countries, our country has not yet made the choice to go towards thermodynamic solar.

Thermoelectric technologies exist in abundance, however, their competitiveness requires greater confidence on the part of governments and private structures in order to promote their implementation and to encourage a reduction in costs through economies of scale. Very briefly, the principle of thermoelectricity is to concentrate the direct solar radiation to generate a heat source at high temperature and then use the temperature gradient between this heat source and the surrounding environment to power a thermodynamic machine. This machine, coupled to an alternator, produces electricity. The first condition to exploit, in an economically profitable way, this technology is to have a sufficient annual normal direct sunshine. BREYER estimates that the minimum threshold can be 1800 kWh/m²/year for the least expensive technologies [5]. With an average sunshine of 5.5 kWh/m²/day for a sunshine duration varying from 3000 to 3500 h/year, Burkina Faso has one of the largest solar deposits in the world [6]. In fact, in Burkina Faso, the average daily incident shortwave solar radiation has a slight seasonal variation throughout the year. The brightest period of the year lasts 2.6 months, from February 11 to April 28, with incident shortwave solar radiation per square meter exceeding 6.2 kWh. The brightest day of the year is April 3, with an average of 6.5 kWh. The darkest period of the year lasts 2 months, from July 14 to September 15, with incident shortwave solar radiation per square meter less than 5.4 kWh. The darkest day of the year is August 17, with an average of 5.1 kWh [7].

In this paper, the heat exchanges that took place in the CPC were presented and explicit expressions for the mass of water vapor produced, the mass flow rate of the water vapor, the saturating vapor pressure and the thermal efficiency were established. Finally, a comparison between theoretical and experimental results was also presented.

2. Materials and Methods

The experimental prototype is installed on the platform of the central maintenance workshop of the University of Joseph KI-ZERBO. The Figure 1 presents the photograph of the device designed to carry out the experimental study.

The descriptive diagram of the test bench is shown by Figure 2.

A data acquisition system "Midi logger GL200A" allows to collect up to 10 values simultaneously, these values are voltages expressed in volts. A calibration allows to convert the voltages in the unit of the measured values (°C). The data can be recorded on a computer or on a USB support. The values recorded by the acquisition system are then extracted in ".csv" format allowing their conversion and analysis on an Excel spreadsheet.



Figure 1. The experimental device prototype.

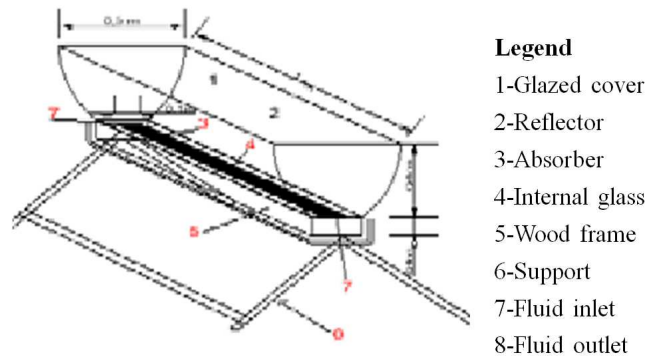


Figure 2. Schematic diagram of experimental setup.

Data acquisition is programmed over a day with a time step of 5 minutes. The values obtained are used to calculate the temperatures. This finally allows drawing the curves of temperatures evolution by time.

The various tests carried out have started since 2017 during the period of strong sunshine in Burkina Faso from March to May of each year. The duration of the experimentation is 10 hours from 8:00 am to 06:00 pm. At the beginning of each experiment, the device is filled with water. There is no water circulation inside the collector because we have chosen a single daily filling boiler which is comfortable from the point of view of the control of the collector, but it is penalizing on a thermal plan because it increases a lot the hot surfaces which lose heat. Contrary to

the boiler of smaller diameter which must be fed manually and several times during the day with a small pump, but which has less inertia and less losses; If the collector is used continuously, this intermittent supply temporarily lowers the temperature / pressure of the steam produced.

Verification is done by direct reading of the different temperatures on the data acquisition. At the end of the day the data acquisition is unloaded on a microcomputer where the digital data are recorded for the different treatments.

3. Modeling of the CPC

3.1. Simplifying Assumptions

The heat balance equations that will be established in the following are based on the following simplifying assumptions:

1. The flow is unidirectional and the regime is assumed to be transient;
2. The conditions are homogeneous on a section of the collector perpendicular to the flow;
3. The edge effects are negligible;
4. Conduction in the glass is negligible;
5. The canopy and the glass are assimilated to a gray body;
6. The sky is assimilated to a black body for a radiation of wavelength taken at the temperature of the sky vault;

7. The ambient temperature is the same at the front and at the back;
8. The effects of dust and dirt on the glass cover are negligible;
9. The portion of the collection area covered by the edges of the sensor is neglected;
10. The air velocity and absolute humidity remain constant along the collector;
11. The thermophysical properties of the air depend linearly on the temperature;
12. Lateral and backward heat transfers are assumed to be negligible;
13. Vertical and axial heat conduction are assumed to be negligible and each component is represented by a single temperature;
14. The external and internal convective exchange coefficients are assumed to be constant over the entire length of the collector;
15. Pressure losses are neglected;
16. The fluid flow rate is assumed to be constant.

3.2. The Heat Balance Equations of the Collector

3.2.1. At the Canopy Level

The glazed canopy receives direct and diffuse radiation on its upper surface and exchanges by convection and radiation with the surrounding environment [5].

$$M_c C_c \frac{\partial T_c(x,t)}{\partial t} = Q_c(x,t) + (h_{r,c-v} + h_{c,c-v})(T_v - T_c) - h_{r,c-ciel}(T_c - T_{ciel}) - h_v(T_c - T_a) \quad (1)$$

3.2.2. At the Glass Level

In the same way, the energy balance for the glass is given by the relation (2) [5]:

$$M_v C_v \frac{\partial T_v(x,t)}{\partial t} = Q_v(x,t) + h_{r,p-v}(T_p - T_v) - h_{c,c-v}(T_v - T_c) - h_{r,c-v}(T_v - T_c) \quad (2)$$

3.2.3. At the Absorber Level

The energy balance at the absorber is obtained by expression (3) [5].

$$M_p C_p \frac{\partial T_p(x,t)}{\partial t} = Q_p(x,t) - h_{r,p-v}(T_p - T_v) - h_{c,p-f}(T_p - T_f) \quad (3)$$

At the fluid level

The energy balance for the heat transfer fluid circulating in the absorber tube is given by the relation (4) [8]:

$$\rho_f C_f e_f \frac{\partial T_f(x,t)}{\partial t} = -\frac{\dot{M}_f C_f}{l_p} \frac{\partial T_f(x,t)}{\partial x} + h_{c,p-f}(T_p - T_f) \quad (4)$$

3.3. Expressions of the Heat Transfer Coefficients

In order to draw up a complete balance of the transfers that took place in the concentrator, we must consider the flow mode of the fluid and the architecture of the device. In our study, we have neglected the heat transfer by conduction.

Heat transfer coefficients between the canopy and the exterior.

We distinguish two types of heat exchange between the cover and the exterior: one by radiation and the other by

forced and/or natural convection.

The coefficient of exchange by radiation between the canopy and the glass.

The coefficient of exchange by radiation between the sky vault and the glass is given by the following expression:

$$h_{r,c-ciel} = k_B \varepsilon_c (T_c^2 + T_{ciel}^2)(T_c + T_{ciel}) \frac{A_c}{A_p} \quad (5)$$

The coefficient of exchange by convection due to wind.

The exchange coefficient between the external environment and the glass is given by the formula of Mac Adams [9]:

$$h_v = (5.7 + 3.8V) \frac{A_c}{A_p} \quad (6)$$

The transfer coefficient between the cover and the glass.

There are two thermal exchanges between the glass and the cover. One by radiation and the other by convection.

The coefficient of exchange by radiation between the cover and the glass.

The coefficient of exchange by radiation between the cover and the glass is given by the following expression:

$$h_{r,c-v} = \frac{\sigma \varepsilon_c (T_c^2 + T_v^2) (T_c + T_v) \frac{A_c}{A_p}}{\frac{1}{\varepsilon_v} + \frac{A_p}{A_c} \left(\frac{1}{\varepsilon_c} - 1 \right)} \quad (7)$$

The coefficient of exchange by convection between the cover and the glass.

The convective transfer coefficient between the canopy and the glass is given by the relation (8) [10]:

$$h_{c,c-v} = (3,25 + 0,0085 \frac{T_v - T_c}{2D_v}) \frac{A_c}{A_p} \quad (8)$$

With:

$$D_v = \frac{2l_v(e_f + e_{p-v})}{l_v + e_f + e_{p-v}} \quad (9)$$

The transfer coefficient between the glass and the absorber. There is a heat exchange between the glass and the absorber. It is the solar radiation between the glass and the absorber. It is given by the following expression:

$$h_{r,p-v} = k_B \frac{(T_p^2 + T_v^2) (T_p + T_v)}{\frac{1}{\varepsilon_p} + \frac{A_p}{A_v} \left(\frac{1}{\varepsilon_v} - 1 \right)} \quad (10)$$

The convection exchange coefficient between the absorber plate and the fluid.

The heat transfer fluid exchanges heat by convection with the absorber. Correlations have been established for the calculation of the Nusselt number according to the nature of the fluid and the flow regime. In this study, the flow regime is laminar. For the calculation of the Nusselt number, the Mercier correlation is used [6]:

$$A_v = L_v l_v \quad (20)$$

The quantity of heat absorbed by the absorber plate.

Equation (21) gives the quantity of heat absorbed by the absorber plate [7]:

$$Q_p(t) = DNI \overline{\tau_c} \rho_m^{<n> \overline{\tau_v}} \left[\overline{\alpha_p} + \overline{\alpha_p \rho_v \rho_p} \frac{A_p}{A_v} \right] \frac{A_c}{A_p} \quad (21)$$

3.5. Calculation of the Mass of Water Vapor Produced and the Mass Flow Rate of Water Vapor

The quantity of sensible heat or the sensible enthalpy of water at saturation. It is obtained by the relation (22):

$$Q_s = M_{eau} C_{eau} \Delta T = M_{eau} C_{eau} (T_{fe} - T_{ie}) \quad (22)$$

The enthalpy of vaporization or the amount of latent heat of vaporization. It is expressed by equation (23).

$$Q_{vap} = M_{vap} L_{vap} \quad (23)$$

The total enthalpy of the saturated steam or the amount of useful or absorbed heat by the water.

We observe that when the solar radiation is concentrated on the absorbing surface, it transmits a quantity of energy to

$$Nu_f = 4.9 + \frac{0.0606 (Re P_r D_h / L)^{1.2}}{1 + 0.0909 (Re P_r D_h / L)^{0.7} P_r^{0.17}} \quad (11)$$

With:

$$Re = \frac{m_f D_h}{l_p e_f \mu_f} \quad (12)$$

$$P_r = \frac{\mu_f}{\lambda_f} C_f \quad (13)$$

$$D_h = \frac{2l_p e_f}{l_p + e_f} \quad (14)$$

The convective exchange coefficient between the fluid and the absorber plate is given by the relation (15):

$$h_{c,p-f} = \frac{\lambda_f}{D_h} Nu_f \quad (15)$$

3.4. Expressions of Heat Quantities

The quantity of heat absorbed by the canopy.

It is given by the expression (16) [7]:

$$Q_c(t) = DNI [\overline{\alpha_c} + \overline{\alpha_c \tau_c} \zeta_m^{2<n>}] \frac{A_c}{A_p} \quad (16)$$

$$A_c = 2WL \quad (17)$$

$$A_p = L_p l_p \quad (18)$$

The quantity of heat absorbed by the glass.

The quantity of heat absorbed by the glass is given by equation (19) [7]:

$$Q_v(t) = DNI \overline{\tau_c} \rho_m^{<n> \overline{\tau_v}} \left[\overline{\alpha_v} + \overline{\alpha_v \rho_v \rho_c} \zeta_m^{2<n>} \frac{A_v}{A_c} + \overline{\alpha_v \zeta_p \tau_v} \right] \frac{A_c}{A_p} \quad (19)$$

the water. This allows the rise of its temperature and then its vaporization. The power received by the latter is written:

$$Q_u = Q_s + Q_{vap} \quad (24)$$

$$Q_u = M_{eau} C_{eau} \Delta T + M_{vap} L_{vap} \quad (25)$$

It is possible to calculate the power received by the receiver following two methods in order to evaluate the difference between what was sent and what was actually received. This will allow to determine the range of energy that the concentrator can bring to the absorber and also to consider solutions in relation to losses. It is given by the following relationship [11]:

$$Q_{rec1} = n_{opt} DNI A_c \quad (26)$$

If we consider the system (water+solar collector), according to the experimental devices, the energy balance is:

$$Q_{rec2} = Q_u + Q_p \quad (27)$$

Calculation of heat loss.

But once the solar rays have made their way to the receiver above the ambient temperature, it raises its temperature above the ambient temperature. This temperature variation

causes a process of heat loss by convection, radiation and conduction. The corresponding power is given by the following expression [11]:

$$Q_p = U_L(T_p - T_a) \quad (28)$$

Calculation of the mass of water vapor produced.

The mass of water vapor produced is obtained by the relation (29):

$$M_{vap} = \frac{Q_u - Q_s}{L_{vap}} \quad (29)$$

With:

$$Q_u = Q_{rec2} - Q_p = n_{opt}DNIA_c - Q_p \quad (30)$$

So the mass of water vapor produced becomes:

$$M_{vap} = \frac{n_{opt}DNIA_c - Q_p - Q_s}{L_{vap}} \quad (31)$$

Calculation of the mass flow of water vapor.

The mass flow of water vapor is the ratio of the mass of water vapor produced per unit time. It is obtained by the equation (32):

$$\dot{M}_{vap} = \frac{M_{vap}}{tc} \quad (32)$$

4. Theoretical and Experimental Results

The experimental curves were smoothed with a coefficient of determination of R^2 tending to 1 with Excel. The figure shows that the theoretical fluid and absorber temperatures are above the experimental temperatures. The both, theoretical and experimental curves have a bell-shaped curve whose

peak is reached at solar noon and the minimum values are seen at sunrise and sunset. For the four days the evolution of the temperatures is the same, there is no difference in the slopes of the curves.

The results show that the temperature of the collector components depends on the incident solar flux and the surrounding climatic conditions. The theoretical fluid temperature reaches 125°C while the experimental fluid temperature oscillates between 107 and 108°C for an experimental global solar radiation up to 955 W/m² and a maximum ambient temperature of 43°C for the day of April 02, 2021.

The theoretical temperatures overestimate the experimental temperatures also because of the high thermal losses of the designed experimental device. The higher the heat losses, the lower the temperatures. With experimental fluid temperatures that exceed the boiling temperature of water, the system generates water vapor. It is noticeable that the measured temperature values vary from time to time, and this is very often due to the evaporation of the heat transfer fluid, when the temperature of the latter reaches 100 °C. This evaporation causes an increase in pressure inside the circuit containing the heat transfer fluid, and since leaks are inevitable, the expansion of the fluid causes a sudden drop in temperature and pressure.

The influence of the cloudy passages is visible, especially on the temperatures. Indeed, significant values that vary from 24 to a maximum of 110°C are been obtained between 12:30 and 13:00 for the day of April 20. Therefore, the use of parabolic trough concentrators allows to reach very high temperatures. The obtained results are very encouraging for the investment of this type in several industrial fields.

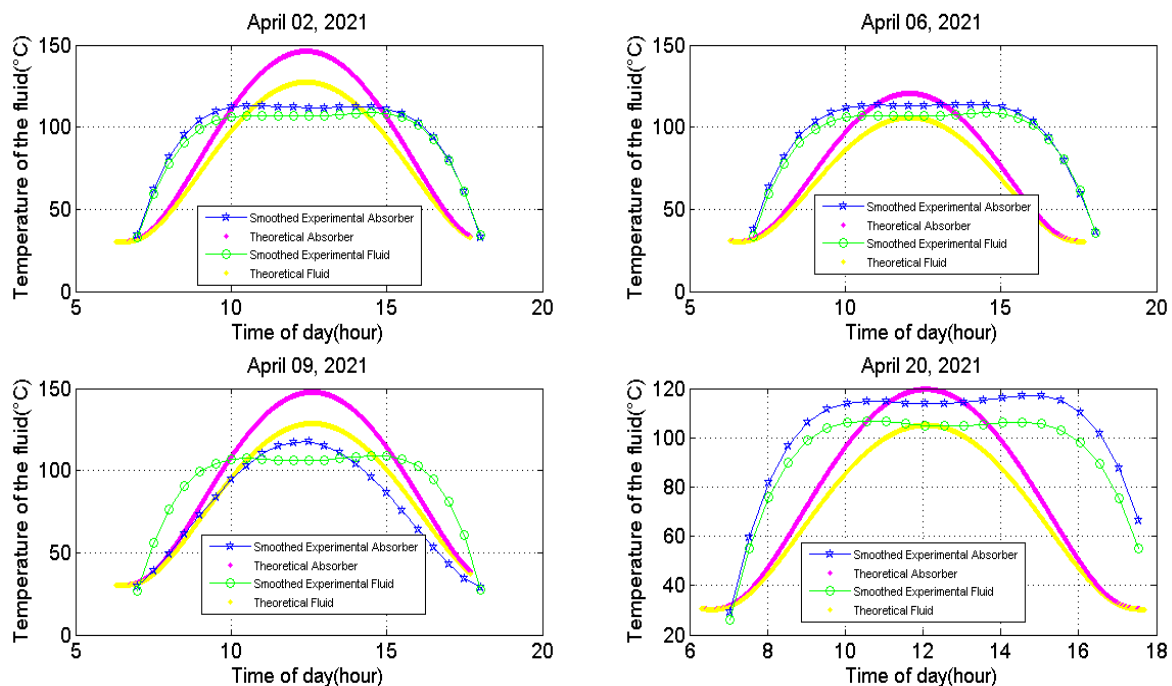


Figure 3. Theoretical and experimental evolution of the fluid and absorber temperatures as a function of time for four days.

Under the effect of sunlight, water is vaporized as saturated vapor at a temperature between 108 and 110°C with a solar aperture area of 0.5 m². Kechidi M. Sayeh and Lazali A. Abbas (2019) measured water and water vapor temperatures in Algeria with a parabolic trough concentrator of 2.40 m length

and 1.20 m width. They obtained 110.7°C for the water temperature and 112°C for the water vapor temperature [12]. Our results are satisfying compared to those obtained by Kechidi M. Sayeh and Lazali A. Abbas. Figure 4 shows the evolution of the temperature of the water vapor.

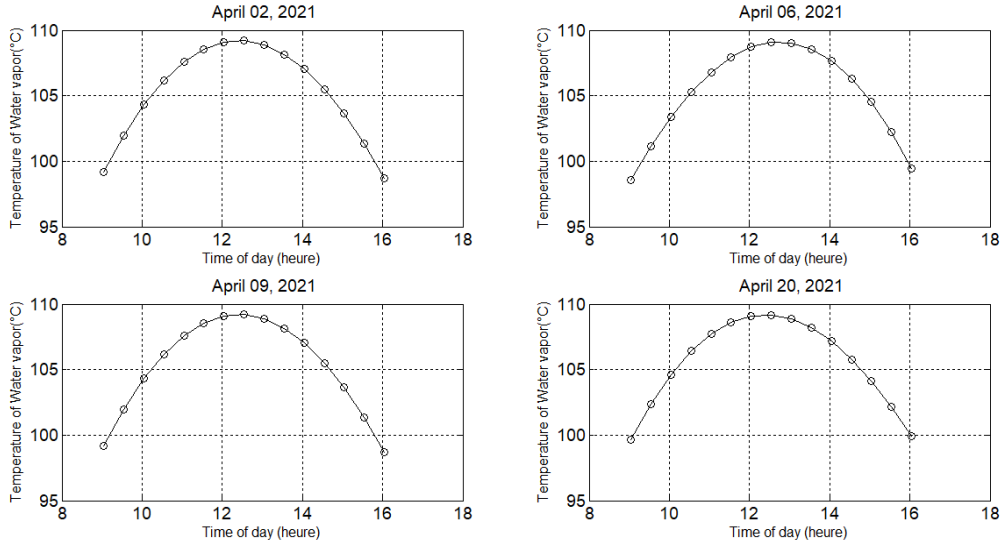


Figure 4. Variations of the experimental temperature of the water vapor as a function of time.

From 8h00 to 9h50mn, corresponds the time of heating of the fluid until reaching the temperature of 100°C. During the heating time of the fluid, there is no production of water vapor. There is only heating heat with a fluid temperature below 100°C. The time taken by the system for the water to reach the boiling temperature is 1h 50 min. This result is close to that of A. Harmin) which is 1h30 min to vaporize 1.5 l of water with an asymmetric CPC [13]. Gudekar et al. experimented with two types of symmetric CPCs. One type with a glass-covered absorber and another without a glass-covered absorber. The covered absorber takes 2.5 hours to vaporize water while the uncovered one takes 1 hour 50 min

to vaporize water. The results of this study are good because they confirm those of Gudekar [14].

Thanks to the manual tracking of solar rays, the system produces water vapor from 9:50 am until 4 pm. During this period the temperature of the fluid is greater than or equal to 100°C. The system is in a state of water-steam mixing with a latent heat of vaporization. The measured steam temperatures oscillate between 108°C and 109°C for the four days with a solar radiation up to 955 W/m² and an ambient temperature around 43°C.

Figure 5 shows the evolution of the theoretical and experimental water vapor mass as a function of time.

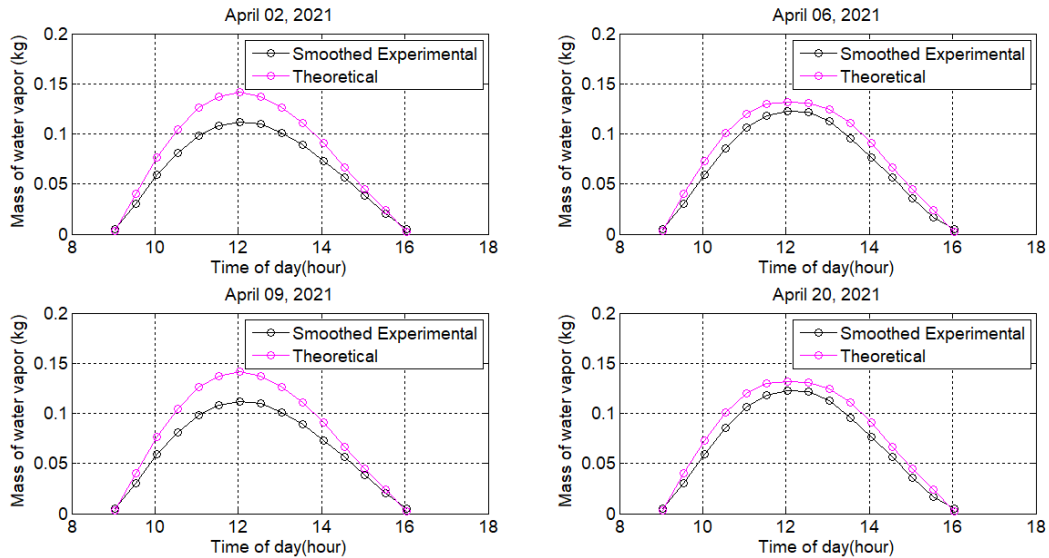


Figure 5. The evolution with time of the theoretical and experimental water vapor mass produced.

With a CPC of 50 cm width and 1m length the theoretical water vapor mass takes the maximum value of at 0.15 Kg at solar noon against 0.110 Kg of experimental water vapor mass for an initial water mass of 1.5 kg of water. The mass of water vapor produced experimentally is small. It depends on the temperatures of the CPC components. The theoretical value overestimates the experimental value of the produced water vapor mass. The above mentioned heat losses also explain this difference between the theoretical and experimental water vapor mass.

Figure 6 shows the theoretical and experimental evolution of the water vapor mass flow rate as a function of time. The

maximum theoretical mass flow rate is reached at solar noon and takes the value of 3.5×10^{-6} Kg/s while the maximum experimental mass flow rate is 3×10^{-6} Kg/s for the day of 02 and 09 April 2021. The experimental mass flow rate is low compared to the theoretical mass flow rate. The results obtained by FALIBAILE showed that with a water mass flow rate equal to 2.77×10^{-4} Kg/s, the parabolic concentrator can vaporize a vapor mass flow rate equivalent to 231×10^{-6} Kg/s [10]. The results of this study are satisfactory even if its results are higher than these one. This can be explain by the fact the parabolic concentrator has a higher optical concentration factor than the parabolic trough concentrator.

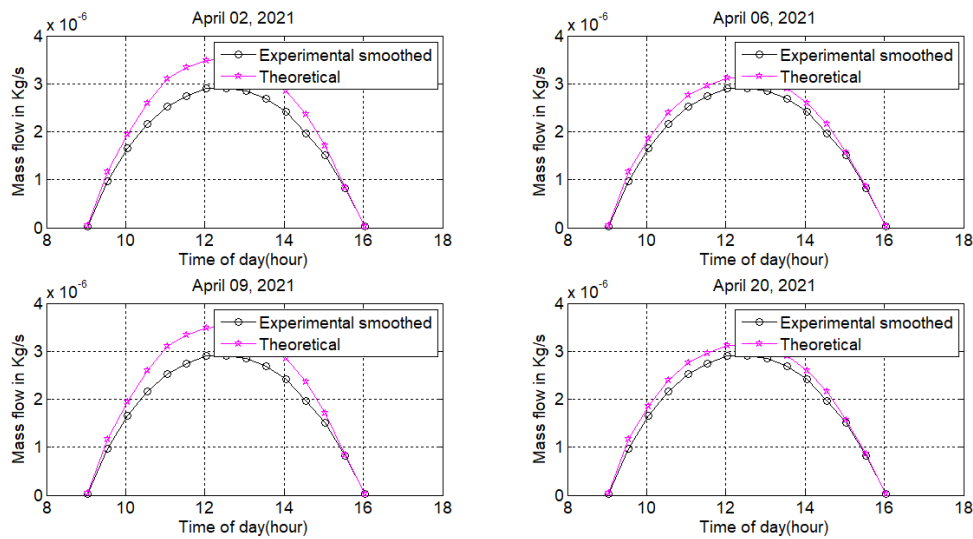


Figure 6. Theoretical and experimental evolution of the water vapor mass flow rate as a function of time.

Figure 7 shows the theoretical and experimental evolution of the saturating vapor pressure as a function of time. The analysis of the figure reveals that at solar noon the theoretical saturating vapor pressure takes the maximum value of 1.25 bars while the maximum experimental saturating vapor pressure is 1.05 bar which is low compared to the theoretical

one for the days of 02 and 09 April 2021. This difference can be explained by the difference between the theoretical temperature of the fluid and the experimental one since there is a relationship between the saturating vapor pressure and the temperature. Thus, the higher the temperature of the fluid, the higher the saturating vapor pressure.

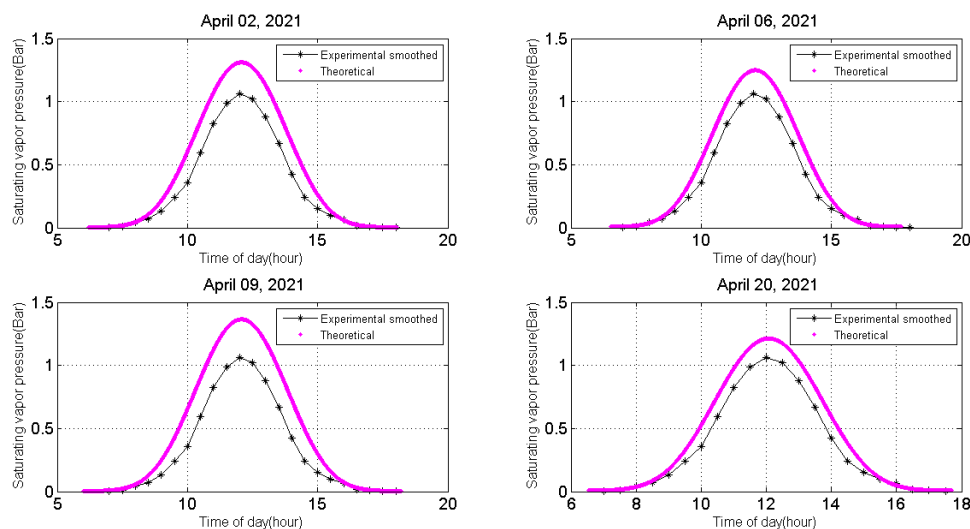


Figure 7. Theoretical and experimental saturation vapor pressure as a function of time.

Figure 8 shows the theoretical and experimental variation of the thermal efficiency as a function of time.

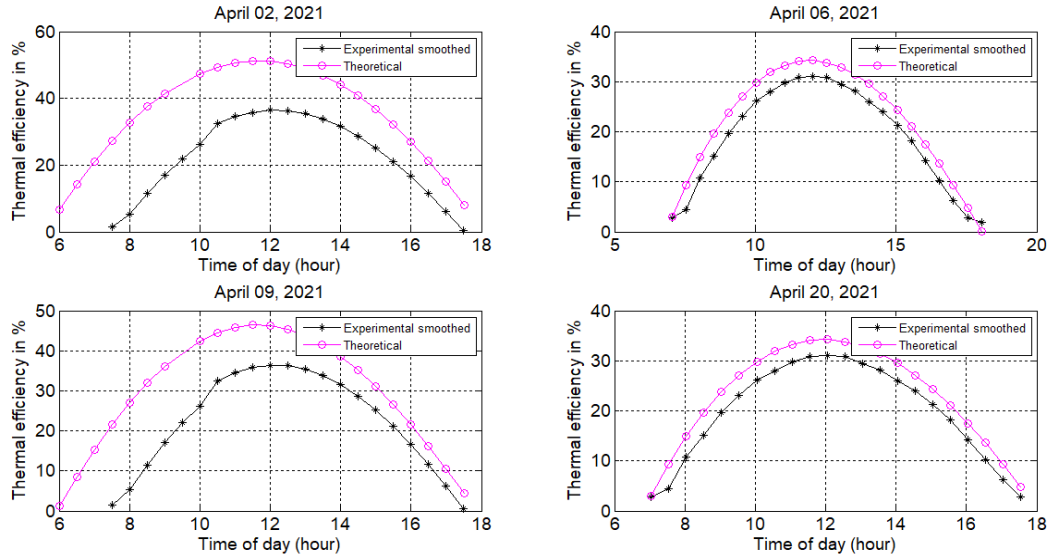


Figure 8. Theoretical and experimental variations of CPC thermal efficiency as a function of time for four days.

Figure 8 above shows that the maximum theoretical thermal efficiency is 52% compared to a maximum experimental thermal efficiency of 35% at most for all four days. The achieved thermal efficiency is appreciable compared to that obtained by Hareth (2019) which is 26.5% using a flat absorber CPC experimented in Mosul, Iraq [15]. All the curves show that the theoretical efficiency is higher than the experimental one.

5. Conclusion

From this paper, it is shown that it is possible to produce steam in a short circuit using the compound parabolic trough concentrator (CPC). The measured steam temperatures can reach 108°C and 110°C respectively with a CPC of length $L_c=1\text{m}$, width $l_c=50\text{ cm}$. The mass of water vapor produced with this device is 0.110 Kg with a mass flow rate of 3×10^{-6} Kg/s and a saturating vapor pressure of 1.05 bar for a global solar radiation of 950 W/m^2 and an ambient temperature of 43°C at solar noon in April 2021. The double-glazed, flat absorber CPC allows for low-cost solar radiation water vapor generation from 9:30 a.m. to 4:00 p.m., an operating time of nearly 7 hours. The CPC is designed to operate only during the day, and we are planning to add a heat storage system to our CPC for night use of the steam produced. In addition, instead of water, we can test the CPC's operation in the future with vegetable oils such as moringa oil, for example.

Nomenclature

Dimensioned numbers

Gr: Grashoff number
Nu: Nusselt number
Pr: Prandtl number
Re: Reynolds number

Greek letters

α : The absorption coefficient

ε : The emissivity

ζ : The reflectance coefficient

η : The efficiency of the concentrator

ϑ : The density, kg m^{-3}

ρ : The specific heat, $\text{J kg}^{-1} \text{K}^{-1}$

τ : The transmission coefficient

Latin letters

A: Surface area, m^2

C: The heat capacity, $\text{J kg}^{-1} \text{K}^{-1}$

e_f : The distance between the bottom of the collector and the absorber plate, m

e_{p-v} : The space between the absorber plate and the glass, m

h: The transfer coefficient, $\text{W m}^{-2} \text{K}^{-1}$

l: The width, m

L: The latent heat of vaporization, $\text{J kg}^{-1} \text{K}^{-1}$

M: The mass of the body, kg

\dot{M} : The mass flow rate, kg s^{-1}

n: The average reflection number

P: The pressure, bar

Q: The quantity of heat absorbed, J

Q_p : Power lost, W

T: The temperature, °C

t_c : Heating time, s

V: Wind speed, m/s

Indexes

c: Covered

c, c-v: Convective between the cover and the glass

c, p-f: Convective between the absorbing plate and the fluid

f: Fluid

fe: Finale

ie: Initiale

p: Absorbing plate

v: Glass

vap: Water vapour

u: Useful

r, c-v: Radiative between the canopy and the sky
 r, c-sky: Radiative between the canopy and the sky
 r, p-v: Radiative between the absorbing plate and the glass

Acronyms
 CPC: Compound parabolic trough concentrator
 DNI: Direct normal radiation, Wm^{-2}

Appendix

Table 1. Characteristics of the hub.

Component	Symbol	Value
Acceptance angle ($^{\circ}$)	θ_c	30
Canopy width (m)	W	0,25
Canopy length (m)	L_c	1
Canopy thickness (m)	ep_c	0,002
Length of glass (m)	L_c	1
Width of the glass (m)	l_v	0,12
Thickness of the glass (m)	ep_v	0,002
Width of the absorber (m)	l_p	0,10
Absorber length (m)	L_p	1
Absorber thickness (m)	ep_p	0,002
Thickness of the insulator (m)	ep_{is}	0,005

Table 2. Thermophysical properties of reflectors.

Physical properties	Symbol	Value
Reflectance of the reflectors	ρ_m	0,92
The reflectance of the canopy	r_c	0,05
Reflectance of the flat absorber	r_p	0,15

Table 3. Thermophysical properties of the glass.

Physical properties	Symbol	Value
Density (kg.m^{-3})	ρ_v	1375
Mass heat capacity ($\text{J.kg}^{-1}.\text{K}^{-1}$)	C_v	840
Thermal conductivity ($\text{W.m}^{-1}.\text{K}^{-1}$)	λ_v	0,0263
Absorption coefficient of the glazing	α_v	0,05
Transmission coefficient of the glazing	τ_v	0,95

Table 4. Thermophysical properties of the absorber.

Physical properties	Symbol	Value
Density (kg.m^{-3})	ρ_p	8900
Mass heat capacity ($\text{J.kg}^{-1}.\text{K}^{-1}$)	C_p	398
Thermal conductivity ($\text{W.m}^{-1}.\text{K}^{-1}$)	λ_p	384
Absorption coefficient of the absorber	α_p	0,98

Table 5. Thermophysical properties of the insulation.

Physical properties	Symbol	Value
Density (kg.m^{-3})	ρ_{is}	322,4
Mass heat ($\text{J.kg}^{-1}.\text{K}^{-1}$)	C_{is}	272
Thermal conductivity ($\text{W.m}^{-1}.\text{K}^{-1}$)	λ_{is}	0,108
Thermal Effusivity ($\text{J.m}^{-2}.\text{K}^{-1}.\text{s}^{-1}$)	F	178

Table 6. Thermophysical characteristics of water.

Characteristic	Formula	Unit
Density of water	$\rho_f = 1001.1 - 0,0867T_f - 0,0035T_f^2$	-
Heat capacity	$C_{pf} = 4196.35 - 0,81714T_f + 0,00934T_f^{-2} + 10^{-5}T_f^{-3}$	($\text{J/Kg}^{\circ}\text{C}$)
Thermal conductivity of water	$\lambda_f = 0,569 + 0,185 \cdot 10^{-2}T_f - 0,749 \cdot 10^{-5}T_f^{-2}$	($\text{W/M}^{\circ}\text{C}$)
Dynamic viscosity	$\mu_f = (17.199 - 0,3389T_f + 0,002T_f^2) \cdot 10^{-4}$	
Latent heat of vaporization	$L_v = 2500 - 2.48T_f$	(KJ/Kg)

References

- [1] ZONGO, S. A., etude de processus physique et chimiques mis en jeu lors de la combustion des huiles vegetales pures dans les moteurs diesels: mecanismes de decomposition et de polymerisation. 2015, Université de Ouagadougou et Université d'Orléans. p. p. 166.
- [2] Grass, Z. M. a. M., Propects and Challenges of Biofuels in Develloping Countries in Conference on International Agricultural Research for Deveolpment University of Kassel-Witzenhausen and University of Göttingen Tropentag 2007: p. p. 17.
- [3] Sven Sielhorst, J. W. M., and Don Offermans Les biocarburants en Afrique: Une évaluation des risques et avantages pour les zones humides d'Afrique. WetLands International, 2008.
- [4] l'Energie, M. d., Tableau de Bord 2017 2018.
- [5] Breyer, C., GLOBAL ENERGY SUPPLY POTENTIAL OF CONCENTRATING. 2009: p. 15-18.
- [6] Plan d'action national des energies renouvelables (PANER). Ministere des Mines et de l'Energie, BURKINA FASO, 2015.
- [7] Mezbahur. Rahman, et al., method of product spacings parameter estimation for beta inverse weibull distribution. Far East Journal of Theoretical Statistics, 2016. 52.
- [8] R. Tchinda, solved the governing equations of the energy to predicted the performance of air heater collector with the CPC having an absorber with flat plate. 2008.
- [9] DUFFIE. J. A., B. W. A., Solar engineering of thermal processes, ed. é. 2nd. 1991, Wiley.
- [10] Hsieh, C. K., Thermal analysis of CPC collectors. Elsevier Ltd, January 1981, Department of Mechanical Engineering, University of Florida.
- [11] FALIBAILE. N, Etude de la production de la vapeur d'eau à partir d'un concentrateur parabolique 2011, 2iE: Ouagadougou.
- [12] Kechidi Mehdi SAYEH, L. A. A., Etude expérimentale d'un concentrateur cylindro-parabolique. 2019, Univerisité Saad Dahlab de Blida 1: Algérie.
- [13] A. Harmim, M. M., M. Boukar and M. Amar Design et test expérimental d'un concentrateur parabolique composé non-symétrique pour la cuisson solaire Revue des Energies Renouvelables 2011. Vol. 14 N°4 (2011) 591–600.
- [14] A. Gudekar, A. J., S. Panse, B. Pandit, Cost efective design of Compound collector for steam generation. 2013.
- [15] Hareth Maher Abd, O. R. A., Firas Aziz Ali and Mothana M. Mohamed Salih, Experimental Study of Compound Parabolic Concentrator with Flat Plate Receiver. 2019.